Experimental study of the jamming transition at zero temperature

Xiang Cheng*
The James Franck Institute and Department of Physics, The University of Chicago, Chicago, Illinois 60637, USA
(Received 17 May 2009; revised manuscript received 16 November 2009; published 9 March 2010)

We experimentally investigate jamming in a quasi-two-dimensional granular system of automatically swelling particles and show that a maximum in the height of the first peak of the pair correlation function is a structural signature of the jamming transition at zero temperature. The same signature is also found in the second peak of the pair correlation function, but not in the third peak, reflecting the underlying singularity of jamming transition. We also study the development of clusters in this system. A static length scale extracted from the cluster structure reaches the size of the system when the system approaches the jamming point. Finally, we show that in a highly inhomogeneous system, friction causes the system to jam in series of steps. In this case, jamming may be obtained through successive buckling of force chains.

DOI: 10.1103/PhysRevE.81.031301 PACS number(s): 81.05.Rm, 61.43.Fs, 83.80.Fg

I. INTRODUCTION

Glasses return to the liquid state upon heating—they become soft and can flow. Sand flowing through a pipe or out of an orifice can easily jam and become rigid. In fact, large classes of materials, ranging from polymer melts to foams, from glasses to dense colloidal suspensions and granular matter, show a similar transition between a flowing liquidlike state and a nonequilibrium disordered solid state. How to understand the nature of this transition is one of the central questions in different fields of materials science [1–5]. The recently proposed jamming phase diagram provides an approach to unify this effort [6,7]. In such a phase diagram [Fig. 1], athermal systems such as granular media sit in the inverse-density $(1/\phi)$/shear-stress (Σ) plane, and thermal systems, such as glass-forming liquids, sit in the inverse-density $(1/\phi)$/temperature (T) plane. When decreasing the temperature, decreasing the shear stress or increasing the density, a system goes from an unjammed phase into a jammed state. At the jamming transition, a material becomes rigid and loses its ability to explore the entire phase space efficiently; it therefore falls out of equilibrium.

Due to its clean and clear signature, jamming along the $1/\phi$ axis in the jamming phase diagram, at zero temperature and zero shear stress, has so far attracted the most attention in simulations and theoretical studies [7–17]. At the zero-temperature jamming point for frictionless spheres (called point J) one observes the onset of rigidity along with other interesting phenomena such as the divergence of the pair correlation function and the appearance of soft modes [7–13,15]. It has been hypothesized that the properties of point J will influence the jamming transition also nearby, similar to critical points in second-order phase transitions. Indeed, it has been found recetly that the signature of the jamming transition at zero temperature shows its vestige at finite temperature [18,19]. Although there has been intensive theoretical and simulation work, only a few experiments have been conducted to study the nature of the zero-temperature jamming transition [20–22]. Especially, the structural signature of the jamming transition has not been directly addressed in experiments by far. Corwin *et al.* probed the structural signature of the jamming transition indirectly at zero temperature along the Σ axis of the jamming phase diagram [23]. Can one directly observe the structural signature of a zero-temperature jamming transition along the $1/\phi$ axis experimentally? How is the picture of jamming modified in a real system with frictional interactions? This paper investigates these essential questions.

Here, we study the zero-temperature jamming transition experimentally in a quasi-two-dimensional granular system of macroscopic particles. By continuously and uniformly increasing the packing fraction, the system is forced to go through the zero-temperature jamming point. In this process, we find a structural signature, which is shown as a maximum of the height of the first peaks of pair correlation function. A similar signature was previously seen in a colloidal sample at nonzero effective temperature [18,19]. Here, we observe a maximum in the second peak as well and, by measuring the pressure on the boundary of system, we show that these features coincide with the onset of rigidity. We also find that *en route* to the jammed phase, our athermal system always self-organizes itself into a structure consisting of particle clusters. A static length scale can be extracted from this structure; it

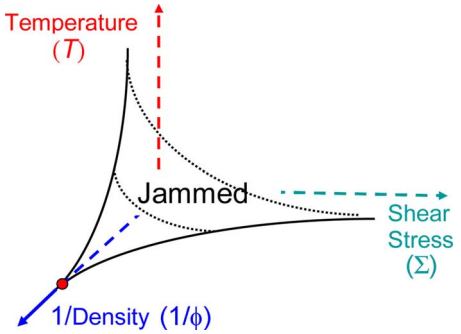

FIG. 1. (Color online) Jamming phase diagram [6,7]. The volume bounded by the black lines near the origin is the jammed phase. When a material crosses the black line from the outside, it goes through the jamming transition. The jamming point along the $1/\phi$ axis, point J, is marked by a red dot.

*Present address: Department of Physics, Cornell University, Ithaca, New York 14853, USA; xc92@cornell.edu

varies between a few particles to the size of the system when the jamming point is approached. Finally, we show that friction can result in multiple jamming points in the presence of highly heterogeneous particle arrangements. A system with friction shows a clear historical dependence. Frictional effects are shown to be reduced or eliminated when small amplitude vibrations are introduced.

II. EXPERIMENTAL METHOD

The granular material used consists of tapioca pearls, which are spherical particles made of starch [Fig. 2(b), inset]. The average diameter of *dry* pearls is 3.3 mm and the cumulative distribution of the sizes of dry pearls is shown in Fig. 2(a). The polydispersity of the pearls is 8%. Such a spread in size is essential to avoid crystallization in a two-dimensional (2D) system. One important property of tapioca pearls is that, when submerged in water, they uniformly expand in size [Fig. 2(b)]. The final diameter of a tapioca pearl can be 1.7 times larger than its original value. The swelling process is very slow. It takes 24 h for a pearl to reach its final fully swelled state. Thus, the system is quasistatic. During swelling, particles keep their approximately spherical shape. The contact interaction between *fully* swelled particles is purely repulsive and of Hertzian type [Fig. 2(c)]. The strain versus stress curve on an individual particle is measured with an Instron System (Model 5869): a particle is put between two horizontal metal plates and the normal force on the top plate is measured while the gap between the two plates decreases. For particles which are not fully swelled, the interparticle contact is still purely repulsive but may deviate from Hertzian form. Some particles may also show slightly plastic deformation.

At the beginning of an experimental run, we put tapioca pearls randomly into a square cell submerged in water. The schematics of the setup can be seen in Fig. 3. Two different sizes of cells are used. The side length of the larger cell is $L=54.6$ cm, which can hold over 15 000 particles with initial packing fractions $\phi_{\text{initial}} \gtrsim 0.63$ (among which about 10 000 particles are studied in the central area to avoid the boundary effect); the side length of the smaller cell, which can contain roughly 2000 particles with about 1000 particles in the central area, is $L=16.5$ cm. In the small cell, we installed a force sensor (Futek load cell, Model LSB200) along one of its sides so that the force or pressure along that boundary can be measured. For both the large and small cells, the gap between the top and bottom plates is kept by a 5.2 mm spacer enclosing the entire boundary. To allow water to flow in and out of the cell, a few thin washers (0.254 mm in thickness) are put on top of the spacer. The total gap thickness (spacer+washer=5.454 mm) prevents fully swelled particles from buckling out of the plane significantly to form two layers. The cell can also be coupled to a mechanical shaker at the bottom, which can vibrate the entire cell vertically. However, unless explicitly indicated, the experiments described here are done without shaking. Vibration is only introduced at the end of Sec. V for controlling the friction between particles. An image of the particles is recorded by a camera mounted above the cell. For a system to reach its fully jammed stationary state, a typical experiment takes between 17 and 24 h. An image was taken every 20 s, so that 3000 to 4000 images were recorded for each experiment. From these images, the center and trajectory of individual particles were extracted.

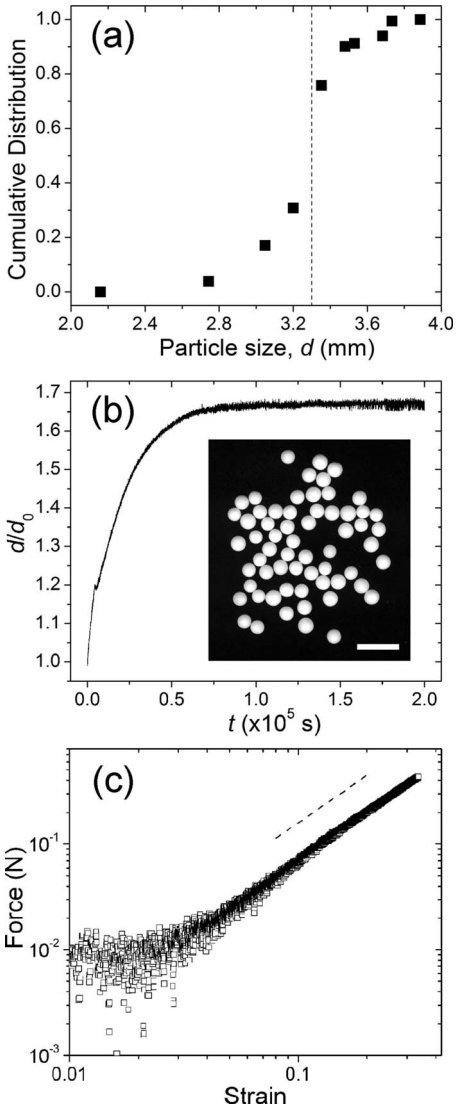

FIG. 2. Properties of tapioca pearls. (a) Cumulative distribution of diameter of dry tapioca pearls. The vertical dashed line marks the average diameter of pearls. (b) Diameter of a swelling pearl under water relative to its original size as a function of time. Inset: optical image of dry tapioca pearls. The white scale bar is 1 cm. (c) Compression force on a fully swelled tapioca pearl as a function of its strain. The strain is defined as $\Delta x/d$, where Δx is the deformation of the particle under compression and $d=4.7$ mm is the original size of the swelled particle at zero compression. The slope of the dashed line is 3/2.

We track the center of particles based on an algorithm developed for colloidal systems [24]. The images obtained are first processed with a bandpass filter to eliminate any global intensity variation and the pixel-size noise. This is a standard procedure before tracking the center of particles [24]. The resulting images are then convoluted with a mask consisting of a white disk with radius a little smaller than the

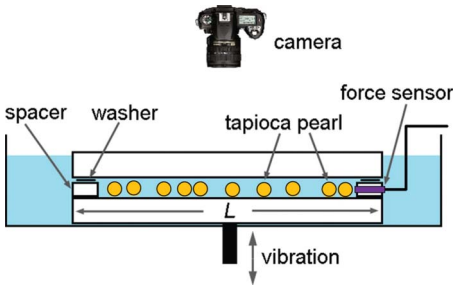

FIG. 3. (Color online) Schematics of the experimental setup. Shown here is the cross section of the cell. The blue (gray) area indicates water.

size of particles. This eliminates any intensity variation on the top surface of individual particles. The local maxima are then located. The center of particles can be found more precisely by calculating the centroid of a blob around each local maximum [24]. The center of particles found in this way is more accurate at early times or low packing fractions. When the system is deep inside jammed phase, the interface between particles has much lower contrast. Therefore, the error of particle tracking becomes larger. When $\phi > 0.90$, about $1-2$ % of particles are missed by the algorithm.

There are several advantages of this system. First, different from other granular systems for studying the jamming transition, where the packing fraction is changed by either changing the number of particles or by changing the volume of system from the boundary [20,25–27], here we can continuously and uniformly increase the packing fraction across the entire system. Second, the system is quasistatic due to the extremely slow swelling of the particles. This allows the static structure of the pack to be easily investigated. Third, after swelling tapioca pearls are much softer than other commonly used granular materials such as glass beads. By assuming the Poisson's ratio of particles around $\sim 1/3$, we can estimate the Young's modulus of swelled particles from the force-strain curve shown in Fig. 2(c). The Young's modulus of swelled tapioca pearls is 0.060 ± 0.005 GPa, which is three orders of magnitude smaller than that of glass beads. Thus, the system can reach far inside the jammed phase. This is essential to directly see any small structural signatures of the jamming transition. With hard granular materials, structural signatures can only be probed indirectly by measuring the contact force distribution between particles [23]. Also, since the entire system is under water, the friction between particles and the bottom plate of the cell is reduced due to lubrication. It is interesting to note that our system is a 2D version of the old experiment done by Hales in 1727 [28,29]. In order to find out how many contacting neighbors a spherical particle has in a dense pack, Hales put peas into a fixed volume container full of water and counted how many dimples each pea had after they had swelled.

III. STRUCTURAL SIGNATURE OF JAMMING TRANSITION AT $T=0$

We initially prepared the 2D samples in a dense, but unjammed phase [Fig. 4(a)]. As the particles become larger, the packing fraction ϕ of the pack increases uniformly across the entire system [Figs. 4(b) and 4(c)]. At a certain moment the system crosses the jamming point and goes into the jammed phase [Fig. 4(d)]. The jamming transition appears to be continuous. The question posed here is whether one can identify the jamming point by looking merely at the structure of the pack.

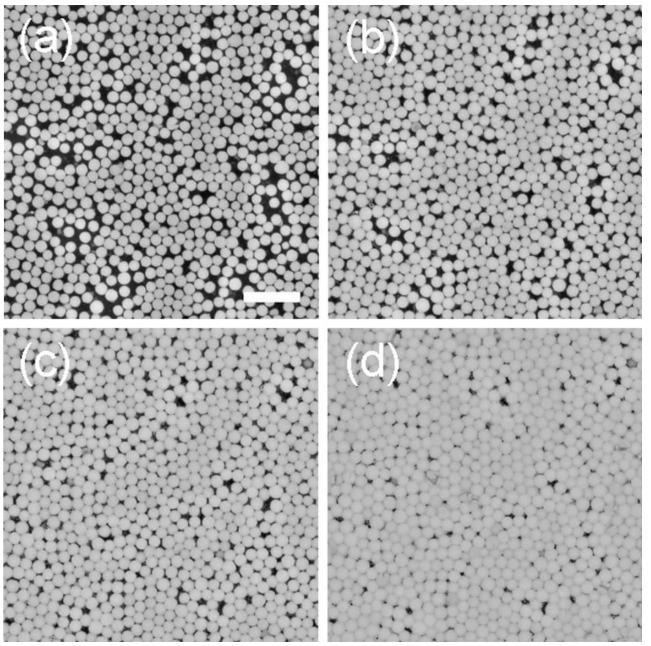

FIG. 4. Jamming transition at zero temperature. The diameter of the particles, and therefore the packing fraction, increases with time. (a) $\phi=0.62$ at $t=0$ h, (b) $\phi=0.76$ at $t=1.10$ h, (c) $\phi=0.84$ at $t=2.81$ h, and (d) $\phi=0.92$ at $t=16.66$ h. The white scale bar is 2 cm.

A. Experimental results

To study the structure of the pack, we measure its pair correlation function $g(r)$ [29]. As shown in Fig. 5, at each ϕ, $g(r)$ has an oscillating shape characteristic of any disordered medium. As ϕ increases from the unjammed phase, the

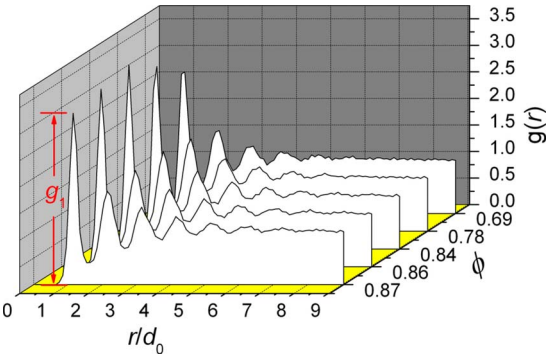

FIG. 5. (Color online) Pair correlation $g(r)$ at different packing fractions. The distance r is given in the unit of the average dry particle diameter d_0. The height of the first peak of $g(r)$, g_1, is indicated.

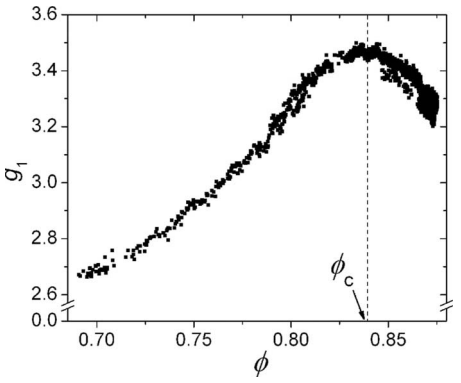

FIG. 6. Structural signature of the jamming transition. The height of the first peak of the pair correlation, g_1, is plotted as a function of ϕ. The position of the maximum is indicated as ϕ_c.

height of the first peak of $g(r)$, g_1, increases first. However, when ϕ is above $\phi_c=0.84\pm0.02$, g_1 begins to decrease [Fig. 6]. Here, we measured the packing fractions from the two-dimensional projection of images. Hence, the average size of particles at ϕ_c can be estimated as $d=d_0(\phi_c/\phi_{\text{initial}})^{1/2}$, where $d_0=3.3$ mm is the average initial size of particles. We identify ϕ_c by fitting $g_1(\phi)$ near its peak with a peak function. Thanks to symmetric shape of $g_1(\phi)$ near ϕ_c, a Gaussian function provides a good fitting. Presumably any other similar peak functions would lead to the same value of ϕ_c. The nonmonotonic trend in $g_1(\phi)$ indicates a structural signature. Is this signature a signature of jamming transition? In other words, is ϕ_c the jamming point?

To answer that, we checked two well-defined criteria for jamming. First, the jamming point is supposed to mark the onset of rigidity in a disordered system [7]: a system composed of particles with finite range purely repulsive interactions at $T=0$ begins to build up pressure on its boundary at this point. As shown in Fig. 7(a), the force measured at the boundary of the cell is zero initially when the system is unjammed and begins to deviate from zero at a ϕ consistent with the peak of g_1. To illustrate the detail of the onset of the jamming, we also plot the force in the logarithmic scale [Fig. 7(b)]. Below the jamming point, the force fluctuates around the noise level (below 100 μN) of the instrument. As ϕ increases further, the slope of the curve changes sharply at $\phi=\phi_c^F$, which is indicated by the left red arrow in Fig. 7(b). Above ϕ_c^F, the pressure on the boundary increases significantly. Note that ϕ_c^F is a little ahead of but very close to ϕ_c. The phenomenon is robust for experiments with uniform initial packing fractions. We find that $\phi_c/\phi_c^F=1.009\pm0.006$, which clearly suggests that ϕ_c, and therefore the structural signature we found in $g_1(\phi)$, is directly related to the jamming transition. We suggest that the small difference between ϕ_c^F and ϕ_c is due to friction in the system. Particles compressed onto the force sensor can be held in a force balance by friction with other particles and with the bottom of the cell, and therefore are not jammed globally with all the particles in the system, which always results in a smaller ϕ_c^F than ϕ_c. However, the static friction in the aqueous system near the isostatic point of the jamming transition is too small to sustain much stress from the swelling of particles. The

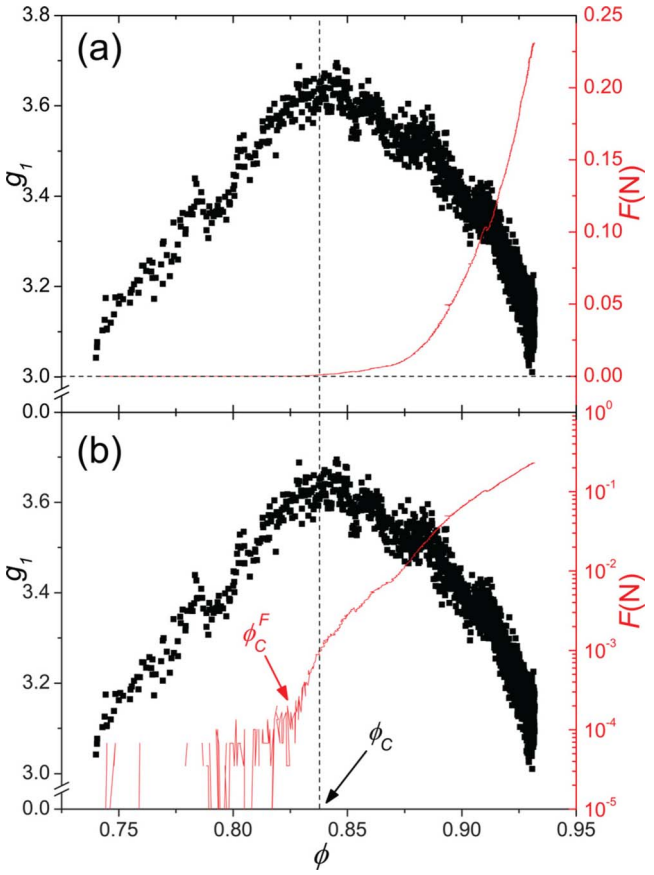

FIG. 7. (Color online) Comparison of the structural signature $g_1(\phi)$ with the force measured along the boundary $F(\phi)$ (a) in a linear-linear plot and (b) in a logarithmic-linear plot. The black squares show $g_1(\phi)$ on the left and the red line shows $F(\phi)$ on the right. The vertical dashed line marks ϕ_c and the horizontal dashed line indicates zero force. The onset of force ϕ_c^F is indicated in (b).

force balance maintained by friction will break down quickly. Therefore, $\phi_c-\phi_c^F\ll1$.

Another supporting evidence is from the motion of particles. Even though the system is athermal, a particle can still be displaced when it touches other particles during the swelling process [Figs. 8(a) and 8(b)]. We shall discuss the displacement of particles in more detail in Sec. IV. Here, it is sufficient to know that the motion of particles stops at the jamming point, which is self-evident as the kinematic criterion of the jamming transition. Ideally, in a homogeneous system, swelling particles will touch the boundaries of the cell in different directions simultaneously, which results in an extremely sharp drop of the average velocity of particles at $\phi=\phi_c$. However, in an inhomogeneous frictional system, some particles may reach a boundary of the cell faster and stop the motion first, while particles in other parts of the system still move. Therefore, there exists a finite interval $\Delta\phi$ for diminishing of particle motion. For an experiment with a uniform initial condition, the interval $\Delta\phi$ is small. To show the average behavior of particles' motion quantitatively, we measured the mean-square displacement of particles, $\langle D^2(\phi)\rangle\equiv\frac{1}{N}\Sigma_{i=1}^{N}|\vec{D}_i(t(\phi))|$, in our experiments. Here, $\vec{D}_i(t(\phi))\equiv\vec{r}_i(t+\Delta t)-\vec{r}_i(t)$ is the displacement of the particle i

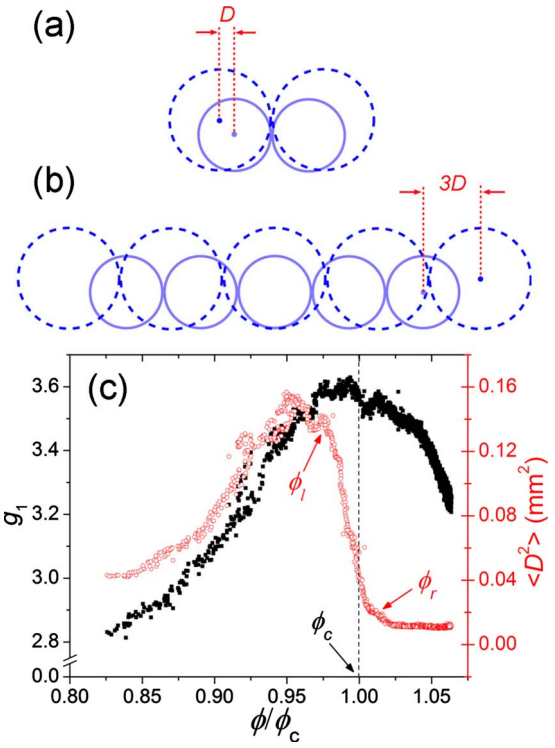

FIG. 8. (Color online) Comparison of the structural signature $g_1(\phi)$ with the mean-square displacement $\langle D^2(\phi)\rangle$. (a) and (b) are sketches to show particle motion. If two particles touch (solid circle), the centers of particles will be displaced after they swelled up (dashed circle). (b) Particles sitting at the edge of a cluster will be displaced most. The displacement is proportional to the size of cluster. (c) Comparison between $g_1(\phi)$ and $\langle D^2(\phi)\rangle$. The displacement of particles D is measured in a time interval Δt=800 s. The black squares show $g_1(\phi)$ on the left and the red circles show $\langle D^2(\phi)\rangle$ on the right. The interval of decreasing $\langle D^2(\phi)\rangle$ is indicated by ϕ_l on the left and by ϕ_r on the right. The vertical dashed line indicates ϕ_c. Due to random noise in the system, $\langle D^2(\phi)\rangle$ does not approach zero at large ϕ. The source of the noise is discussed in the main text of Sec. IV.

at time t within a small time interval Δt [or equivalently at packing fraction ϕ within an interval $\Delta\phi$ since the monotonic dependence of $t(\phi)$] and the summation is over all the particles in the studied area. $\vec{r}_i(t)$ is the center of the particle i at t. We fixed Δt to be a small constant compared with the time scale of the swelling of particles, so $\vec{D}_i(t)/\Delta t$ is approximately the instantaneous velocity of particle i at t. Hence, the mean-squared velocity should show qualitatively the same behavior as that of $\langle D^2\rangle$. Note that the mean-square displacement defined here is different from the more common concept used in studying the diffusion of Brownian particles. The result of $\langle D^2(\phi)\rangle$ is shown in Fig. 8(c). As one can see from the plot, $\langle D^2(\phi)\rangle$ decreases to zero quickly in an interval between ϕ_l and ϕ_r as indicated in the figure. For all experiments with uniform initial packing fraction, we found that $\Delta\phi/\phi_c \equiv (\phi_r - \phi_l)/\phi_c = 0.03 \pm 0.01$. More importantly, ϕ_c is always located between ϕ_l and ϕ_r (i.e., $\phi_l < \phi_c < \phi_r$). This confirms the argument that the structural signature in $g_1(\phi)$ is due to the jamming transition.

Both the mechanical and kinematic measurements show that ϕ_c indeed corresponds to the jamming point of frictional systems. Therefore, the peak in $g_1(\phi)$ manifests the structural signature of the zero-temperature jamming transition. But how can we understand this structural signature? What is the physical or geometric origin of it? We shall discuss it next.

B. Discussion

It is well known that when a molecular liquid goes through glass transition upon decreasing T in the jamming phase diagram, no structural signature can be observed [2,32]; g_1 monotonically increases as the system passes through the glass transition temperature T_g. Then why does g_1 show a peak when the system goes through jamming transition along the $1/\phi$ axis? This was discussed in Ref. [18], where a vestige of the zero-temperature signature was observed in a finite-temperature colloidal system. When ϕ approaches ϕ_c from the unjammed side, particles are pushed closer to each other. Therefore, g_1, which indicates the probability that nearest neighbors of a particle are located at the same distance, increases as the total number of nearby neighbors increases. However, above the jamming transition, particles begin to overlap and deform. Since the degree of deformation depends on the local environment of a particle, the distribution of distances between two particles in contact becomes broader. Meanwhile, the number of nearest-neighbor particles (the coordination number) does not increase appreciably, i.e., the area under the first peak of $g(r)$ remains roughly constant. As a result, g_1, the height of the first peak in $g(r)$, decreases. In simulations with monodisperse frictionless particles, at the jamming point, all particles are precisely one particle diameter away from their nearest neighbors. Hence, g_1 diverges at this point [9]. In our system, the polydispersity of the particles reduces g_1. Even without friction, at the jamming point, the distribution of distance between two particles in contact still has a finite width reflecting the size distribution.

Friction may complicate the situation further. Both the coordination number and the deformation of particles under compression are profoundly changed in the presence of friction as indicated in previous simulation and theoretical works [11,12,30,31]. Hence, it is not straightforward to extend the results of ideal frictionless system on which most simulation and theoretical studies focus [7–10,13,14,16,17] to experiments with real frictional granular matter. Experimentally, Majmudar *et al.* found that the increasing of the coordination number $Z-Z_c$ and the pressure P of the system as a function of $\phi-\phi_c$ agrees with the mean-field theory for frictionless particles [20]. However, the two experiments on the sound propagation near the surface of loosely compacted granular packs show that the ratio of the shear modulus to the bulk modulus, G/B, stays constant rather than diminishing as the pressure of the system approaches zero [21,22], which contradicts to the result of frictionless particles [7,17]. Until now, no direct measurement has been conducted on the structural signature of the jamming transition in a real granular system. Here, we show that structural signature predicted with frictionless particles [9] persists in the system of real

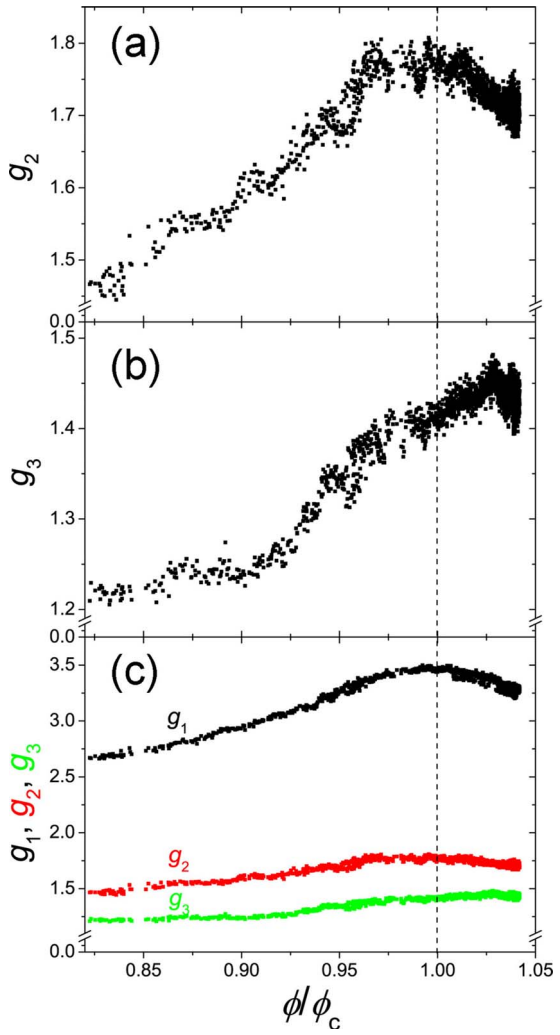

FIG. 9. (Color online) Structural signature in higher-order peaks of the pair correlation function. (a) Height of the second peak of pair correlation function, g_2, as a function of ϕ. (b) Height of the third peak of pair correlation function, g_3, as a function of ϕ. (c) Comparison of the amplitudes of $g_1(\phi)$, $g_2(\phi)$, and $g_3(\phi)$. The vertical dashed line indicates $\phi/\phi_c=1$.

granular matter with frictional contact, although the signature is modified significantly.

Finally, it is also interesting to look for this structural signature in the other peaks of the pair correlation function. The system with the larger cell contains enough particles to show the first four peaks of $g(r)$ clearly [Fig. 5]. As seen in Fig. 9(a), the height of the second peak of $g(r)$, g_2, as a function of ϕ also shows a maximum at the same value of ϕ_c, at which $g_1(\phi)$ shows a maximum. However, the amplitude of this maximum is smaller than that of g_1 [Fig. 9(c)]. One may think that the height of the nth peak of the pair correlation function, g_n, would also show a peak at ϕ_c but with decreasing amplitude as n increases. However, when we measured the height of the third peak, $g_3(\phi)$, no peak is found; instead, g_3 increases rapidly at small ϕ and slows down or plateaus in some cases at large ϕ [Fig. 9(b)]. The structural signature of jamming transition apparently manifests itself in the first and the second peaks of the pair correlation function but not in the peaks at larger separation. As a comparison, in the simulations with frictionless monodisperse particles, the second peak of the pair correlation function splits into two subpeaks [9,29] both of which have a divergent slope [9]. Furthermore, no singular behavior of g_3 is found in simulations [9]. So far, unlike the case of g_1, no clear geometric picture exists for why g_2 should diverge at the jamming point [9]. We speculate that the underlying mechanism for the singularity of simulations may be related to the experimental finding.

IV. FORMATION OF STATIC CLUSTER STRUCTURE

In this section, we investigate the displacement field of the particles. We shall show that, for any typical pack, the system eventually organizes itself into clusters. One can extract a static length scale from the sizes of the clusters. This length grows dramatically from the size of a few particles to the size of the entire system when the system approaches the jamming point.

A. Displacement of particles

The centers of two contact particles separate due to the enlargement of their radiuses as illustrated in Fig. 8(a). Thus, by tracking centers of particles, one can observe clear motion in this athermal system.

Now let us first have a look at the average behavior of particles at different stages through the jamming transition. As shown in Fig. 8(c), the mean-square displacement of particles, $\langle D^2(\phi)\rangle$, shows a nonmonotonic behavior. Since only a few pairs of particles have contacts initially, $\langle D^2(\phi)\rangle$ is small at the beginning [Fig. 8(c)]. As the size of particles increases, more particles form contacts and are displaced; $\langle D^2(\phi)\rangle$ increases correspondingly. When the system approaches the jamming point, almost all the particles join into a contact network, so that $\langle D^2(\phi)\rangle$ reaches a maximum. However, shortly after that, the moving particles begin to touch the boundary and $\langle D^2(\phi)\rangle$ quickly drops toward zero as the entire system jams. The position of the peak $\langle D^2(\phi)\rangle$ is always before the peak of $g_1(\phi)$. Deep inside the jammed regime, there are rare buckling events: particles suddenly change their relative positions on a much shorter time scale than that for particle swelling. These events are discrete and localized—a typical buckling event involves only two to five particles. This is reminiscent of the $T1$ process found in a two-dimensional foam [33].

B. Displacement field and cluster structure

More information can be obtained from the displacement field of the system. To visually illustrate the particle-displacement field, we subtract two images of the system at different times. Any stationary part of the system will appear black in such difference images since the individual pixels are identical in that region. However, if a particle moves, the image subtraction will produce an area of crescent shape with positive values along the front boundary in the moving direction and leave a similar crescent area with negative values in the rear. Furthermore, we assign the negative values to

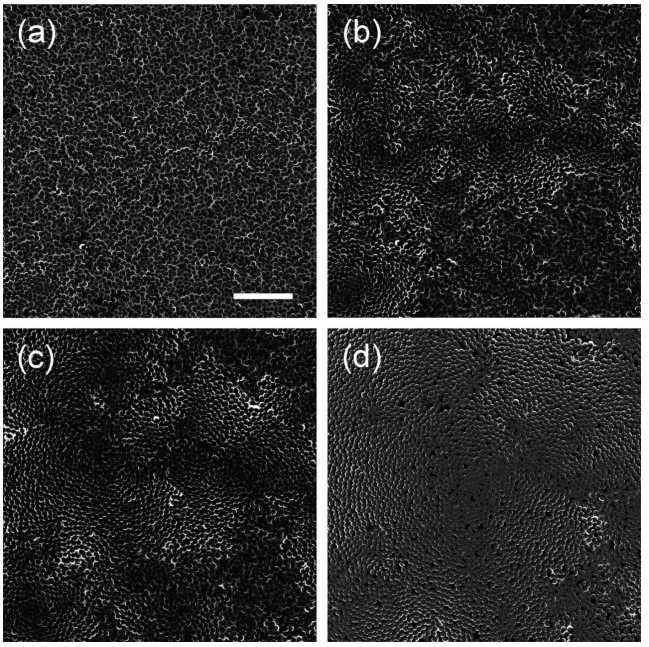

FIG. 10. Cluster structure. Displacement field of a subsystem in the large cell (54.6×54.6 cm^2). The time interval for the displacement is $\Delta t = 800$ s. (a) $\phi = 0.65$ at $t = 0$ h, (b) $\phi = 0.74$ at $t = 1.30$ h, (c) $\phi = 0.79$ at $t = 2.29$ h, and (d) $\phi = 0.84$ at $t = 3.92$ h. The white scale bar is 5 cm.

zero (black). Hence, only front boundaries in the moving direction are indicated in the image. The curvature and area of the crescent show the direction and magnitude of a particle's displacement, respectively [Figs. 10(a)–10(d)].

Figures 10(a)–10(d) show the displacement field of a typical experiment. The displacement field is initially random [Fig. 10(a)]. As the system evolves toward higher packing fractions, a coherent structure emerges [Figs. 10(b) and 10(c)]. Particles tend to move outward around a few nuclei. In other words, a few clusters form in the system. Eventually, when the system approaches the jamming point, one single cluster forms [Fig. 10(d)].

How does the cluster structure emerge out of a random initial configuration? As mentioned above, since only a few pair of particles are in contact initially, the average displacement is small and the directions of displacement are random at the beginning [Fig. 10(a)]. As the size of particles increases, they begin to form local contact networks—cluster structure emerges [Fig. 10(b)]. Encircled by its neighbors, a particle at the center of a cluster feels zero average force due to the balance of the compression from different directions. Hence, it stays in stationary and shows as a dark nucleus in the displacement field [Fig. 10(b)]. Meanwhile, the surrounding particles move away from the center radially. Due to inevitable initial density variations, the denser part of system will form clusters first. Since the displacement of particles at the edge of a cluster is linearly proportional to the size of the cluster [Figs. 8(a) and 8(b)], a larger cluster will grow faster and therefore aggregate more particles. Thus, the clusters formed at early time in the denser part of system will quickly dominate the system and the small initial density variation is amplified. When two clusters meet, the internal particles and

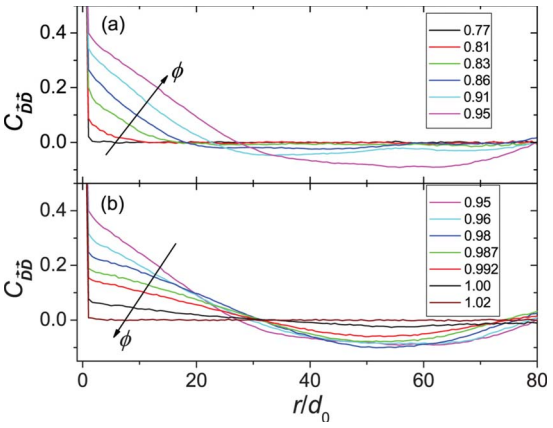

FIG. 11. (Color online) Correlation of the displacement of particles, $C_{\vec{D}\vec{D}}(r)$, (a) before the mean-square displacement reaches the maximum and (b) after the maximum near the jamming point. The arrows indicate the direction of increasing packing fraction. Values of ϕ/ϕ_c are shown in the plots. The time interval for the displacement is $\Delta t = 200$ s.

especially those along the cluster boundaries rearrange and the two clusters merge into a single bigger entity [Figs. 10(b) and 10(c)]. This merging of clusters continues until a single system-spanning cluster forms when the system approaches the jamming point [Fig. 10(d)].

The exact shape of evolving clusters depends on the initial condition of experiments. For the experiment shown in Fig. 10, the initial density is higher in the central area of the system. Hence, the cluster structures appear first in that area and then expand outwardly. Although details depend on a packing's history, the existence and development of cluster structures are robust. Unless over 10 000 particles in the system start out with, and maintain, exactly the same interparticle spacings, which clearly is unrealistic, the system will always evolve into cluster structures at later time. Any small initial density variation will be amplified as the system approaches the jamming point.

C. Quantitative analysis

To quantify the cluster structure, we measure the two-point correlation function of the displacement field,

$$C_{\vec{D}\vec{D}}(r) = \frac{\frac{1}{N_0}\sum_{i,j=1}^{N}[\vec{D}(\vec{r}_i)\cdot\vec{D}(\vec{r}_j)]\delta(r_{ij}-r)}{\frac{1}{N}\sum_{i=1}^{N}\vec{D}(\vec{r}_i)\cdot\vec{D}(\vec{r}_i)}, \quad (1)$$

which is usually used to identify coherent structures in a system. Here, $\vec{D}(\vec{r}_i)$ is the displacement of the particle i located at $\vec{r}_i$ within a small time interval Δt, and $r_{ij} = |\vec{r}_i - \vec{r}_j|$. The summations are over all the N particles in the system and the normalization factor $N_0 = \Sigma_{i,j=1}^{N}\delta(r_{ij}-r)$. Experimentally, the data are binned with a bin size of two thirds of a particle diameter. As one can see in Fig. 11(a), initially at low packing fraction ($\phi/\phi_c = 0.77$) no correlation exists, $C_{\vec{D}\vec{D}}(r>0) = 0$. As the packing fraction increases, clusters be-

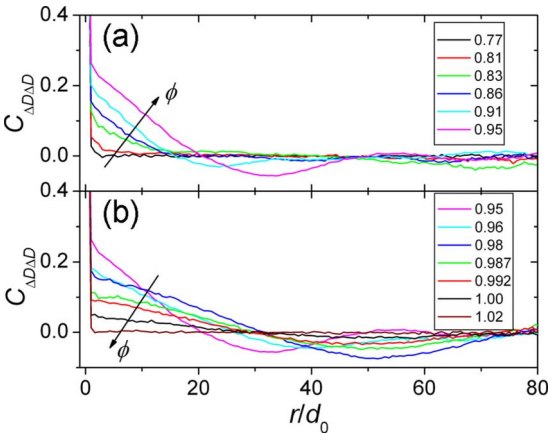

FIG. 12. (Color online) Correlation of the magnitude of particle displacement, $C_{\Delta D\Delta D}(r)$, (a) before the mean-square displacement reaches the maximum and (b) after the maximum near the jamming point. The arrows indicate the direction of increasing packing fraction. Values of ϕ/ϕ_c are shown in the plots. The time interval for the displacement is $\Delta t=200$ s.

gin to form. Correspondingly, both the correlation and the correlation length increase [Fig. 11(a)]. For example, the point where $C_{\vec{D}\vec{D}}$ crosses zero shifts to larger r as ϕ increases. The correlation reaches a maximum when the mean-square displacement $\langle D^2(\phi)\rangle$ is largest. As $\langle D^2(\phi)\rangle$ falls near the jamming point [Fig. 8(c)], the correlation magnitude decreases but the length scale of the correlations is fixed at the size of the system [Fig. 11(b)]. One can of course choose other correlation functions for identifying cluster structures. The correlation function chosen here includes the information of both the direction and magnitude of displacements. We also measure the correlation of only the magnitudes of particle displacement, which is defined as

$$C_{\Delta D\Delta D}(r) = \frac{\frac{1}{N_0}\sum_{i,j=1}^{N} \Delta D(\vec{r}_i)\Delta D(\vec{r}_j)\delta(r_{ij}-r)}{\frac{1}{N}\sum_{i=1}^{N} \Delta D(\vec{r}_i)\Delta D(\vec{r}_i)}, \qquad (2)$$

where $\Delta D(\vec{r}_i)=D(\vec{r}_i)-\langle D\rangle$ is the fluctuation of the magnitude of particle displacement at $\vec{r}_i$. $D(\vec{r}_i)$ is the magnitude of particle displacement and $\langle D\rangle$ is the average magnitude of particle displacement. We show $C_{\Delta D\Delta D}(r)$ at different packing fractions in Fig. 12. As one can see, $C_{\Delta D\Delta D}(r)$ shows qualitatively the same behavior as $C_{\vec{D}\vec{D}}(r)$.

$C_{\vec{D}\vec{D}}(r)$ [or $C_{\Delta D\Delta D}(r)$] shows a clear trend of the increasing of correlation between the displacements of particles. It provides a good qualitative illustration of the emergence and the evolution of cluster structures. However, it is hard to extract the length scale of clusters from this function directly—$C_{\vec{D}\vec{D}}(r)$ does not decrease exponentially with r and there is no obvious feature in $C_{\vec{D}\vec{D}}(r)$. Furthermore, due to the random noise in the displacement of individual particles, the correlation function shows a sharp jump from $C_{\vec{D}\vec{D}}(0)=1$ to $C_{\vec{D}\vec{D}}(r=d_0)$. A particle always perfectly correlates with itself, but the correlation between different particles is reduced due to random noise. Hence, there exists a sharp jump from the self-correlation at $r=0$ to the correlation of neighboring particles at $r=d_0$. The jump is more severe when the signal/noise ratio is smaller at the beginning of the experiment or in the jammed phase [Fig. 11]. (At the beginning, when particles do not touch and at the end when particles are jammed, the signal/noise ratio is ~ 0.) The random noise can be due to the nonuniform swelling of particles. If the shape of a particle changes during swelling, the center of the particle may move slightly even without contact with other particles. The particle-tracking algorithm can also induce some noise. However, that only happens when the system is deep inside the jammed phase where the interparticle spacing is so small that it becomes hard to distinguish the boundary between two neighboring particles.

Another way to quantify the cluster formation is to measure the projection of the relative displacement of two particles on the direction of their relative position [Fig. 13(a)],

$$D_r(r) = \frac{1}{N_0}\sum_{i,j=1}^{N}\left([\vec{D}(\vec{r}_i)-\vec{D}(\vec{r}_j)]\cdot\frac{\vec{r}_{ij}}{r_{ij}}\right)\delta(r_{ij}-r). \qquad (3)$$

The bin size is again chosen as two thirds of a particle diameter. $D_r(r)$ indicates on average whether a pair of particles at separation r moves closer $[D_r(r)<0]$ or moves apart $[D_r(r)>0]$. If there are no clusters and all the particles move randomly, $D_r(r)$ will be zero. However, inside a cluster, any two particles cannot move closer [Fig. 13(a)]. Therefore, in a cluster with size r_0, $D_r(r<r_0)\geq 0$. When all particles are stationary, $D_r(r)=0$. Figure 13(b) shows $D_r(r)$ at different packing fractions. As one can see, initially there is no coherent motion and $D_r(r)$ is flat at zero. However, as the system evolves, $D_r(r)$ begins to deviate from zero and a region with a positive $D_r(r)$ clearly shows up implying the presence of clusters. Although the amplitude of this positive region shows a nonmonotonic behavior, the position of the peak at l increases with ϕ. Thus, l can be used as a characteristic length scale of clusters. As shown in Fig. 13(c), l increases slowly from a few particles diameter at low ϕ and increases rapidly to the size of the system when the system approaches the jamming point. The exact shape of $l(\phi)$ depends on the initial configuration of the particles, but qualitatively all packs show the same behavior.

D. Discussion

In contrast to the length scales determined from dynamic heterogeneities in supercooled liquids [34,35], colloidal suspensions [4,36], and granular media [25–27], the length measured here reflects the static structure of system. One might imagine that the average packing fraction inside a cluster is higher than that outside the cluster. The cluster structure observed here is due to the athermal nature of the system. Clearly, the cluster structure depends on the initial packing configuration. Although we prepare packs in a random way with unavoidable small density variations, the system always amplifies this initial variation into a cluster structure at later time. Such history dependence and memory are typical of nonequilibrium systems [37–39]. On the contrary, in any

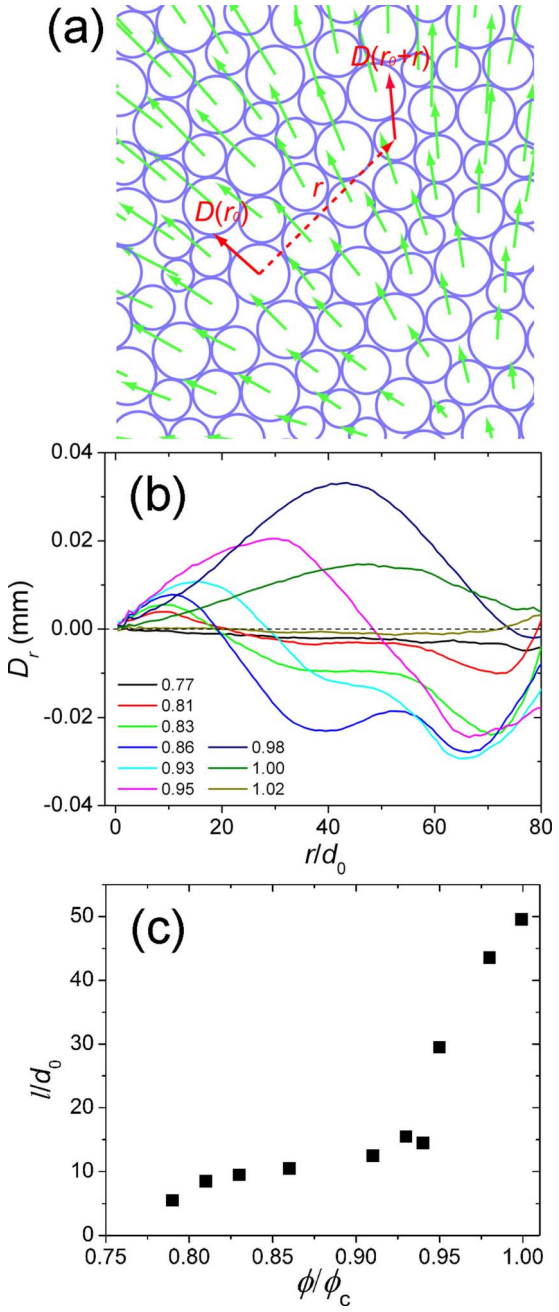

FIG. 13. (Color online) Projection of the relative displacement of two particles on the direction of their relative position D_r and length scale l extracted from the cluster structure. (a) Illustration of the definition of D_r. A pair of particles with distance r (shown with red arrows) always move apart inside a cluster. (b) D_r as a function of r for different packing fractions. The time interval for the displacement is $\Delta t=200$ s. Values of ϕ/ϕ_c are shown in the plot. The horizontal dashed line indicates $D_r=0$. (c) Length scale l extracted from D_r, as a function of ϕ/ϕ_c.

equilibrium system without attraction, the initial density fluctuations will quickly be smeared out; unless the system approaches a second-order phase transition, the correlations of the density fluctuations in equilibrium systems will remain small. The existence of a divergent static length scale in the glass or jamming transitions would be a hallmark for an underlying phase transition. However, until now, no unambiguous static length scale has yet been observed in any equilibrium system near a glass or jamming transition. The present experiment suggests that at the jamming transition a *nonequilibrium* system can produce a divergent static length scale. It should be noted that previous simulation works on the jamming transition at zero temperature acquire the unjammed configuration by quenching the system from $T=\infty$ to $T=0$ [7–11]. Therefore, even though the system is at $T=0$, the static configuration of the system is essentially the same as that at $T=\infty$. Contacts between particles do not exist before jamming and static length scale cannot be found in these simulations.

V. EFFECT OF FRICTION: MULTIPLE JAMMING POINTS

As shown in the above section, the initial density variation—no matter how small it is—will be amplified by the system *en route* to the jammed phase and the system will spontaneously organize into cluster structure. In this section, we shall investigate how this density variation influences the signature of the jamming transition. We shall show that for a system with sufficient large initial density variation, i.e., for a highly inhomogeneous system, friction plays an important role and multiple jamming points exist.

Practically, the initial density variation can be effectively controlled by the total number of particles in the system. If enough particles are added at the beginning, the initial packing fraction of system will be high and the density variation will be small. In this case, although the cluster structure still emerges while the system approaches the jamming point, the system will eventually show a clear jamming transition and therefore an unambiguous structural signature of the transition as shown in Sec. III. However, if the sample is prepared at a low initial packing fraction, due to random vibrations during the sample preparation, there is a good chance that one part of the system is denser than the rest. The initial density variation of the system will be much higher. Hence, we can easily prepare a highly inhomogeneous system by simply reducing the initial packing fraction. With a highly inhomogeneous system at hand, we want to ask how such a system goes through the jamming transition. Is the jamming signature of a highly inhomogeneous system the same as that of a homogeneous system?

Figure 14(a) shows the height of the first peaks of the pair correlation function, g_1, as a function of ϕ for a system with low initial packing fraction (typically $\phi_{\text{initial}} \leq 0.60$). Instead of a single pronounced peak, there are two major peaks located at $\phi_1 \simeq 0.74$ and $\phi_2 \simeq 0.84$ (and possible several smaller peaks). We can compare $g_1(\phi)$ with the mechanical and kinematic criteria of the jamming transition separately. As shown in Fig. 14(a), the pressure on the boundary begins to deviate from zero near the first peak ϕ_1. However, if one compares $g_1(\phi)$ with the mean-square displacement $\langle D^2 \rangle$, one finds that $\langle D^2 \rangle$ drops to zero at the second peak ϕ_2 [Fig. 14(b)]. Therefore, the system jams at ϕ_1 according to the mechanical criterion for the jamming transition and jams at ϕ_2 according to the kinematic criterion. Why do the two

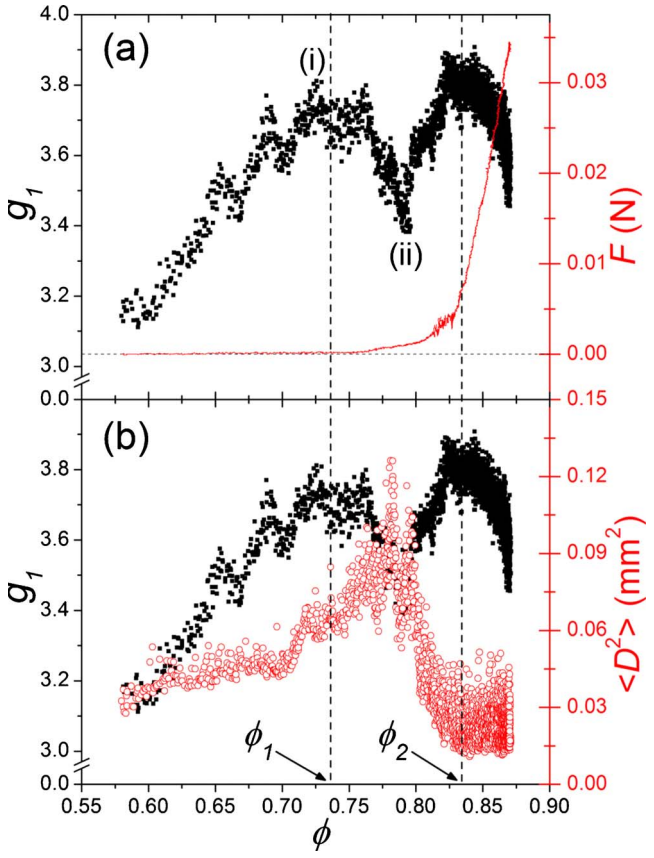

FIG. 14. (Color online) Height of the first peak of the pair correlation function, g_1, as a function of ϕ for a system with low initial packing fraction, and comparison of $g_1(\phi)$ with (a) the force along the boundary $F(\phi)$ and with (b) the mean-square displacement of particles $\langle D^2(\phi)\rangle$. $g_1(\phi)$ is shown on the left with black squares. The vertical lines mark the positions of two major peaks, ϕ_1 and ϕ_2. (i) and (ii) indicates the positions where we show the displacement field in Fig. 15. $F(\phi)$ is shown on the right of (a) with red line. The horizontal dashed line indicates zero force. $\langle D^2(\phi)\rangle$ is shown on the right of (b) with red circles. The time interval for the displacement is $\Delta t = 800$ s.

well-defined criteria for the jamming transition occur at two different packing fractions?

To understand this, we plot the displacement field at two different packing fractions in Fig. 15: (i) at the first peak ϕ_1 [Fig. 14(a)] and (ii) at the valley between ϕ_1 and ϕ_2 [Fig. 14(a)]. As one can see, at ϕ_1 the system already forms clusters [Fig. 15(a)]. From the local mean displacement (red arrows), one can see that the two clusters span the system from left to right. The cluster on the right pushes onto the force sensor at the boundary of cell. Clearly, the system jams and a force chain forms along this direction from left to right. However, there is still empty space in the lower right corner of cell. After the two clusters merge, the particles move together toward the lower right corner as shown in the displacement field near the valley [Fig. 15(b)]. The system jams globally at ϕ_2, which results in the dramatic drop of the mean-square displacement. Therefore, the reason why there are two peaks in $g_1(\phi)$ is that the system jams in two steps: it first jams locally along certain direction (from left to right)

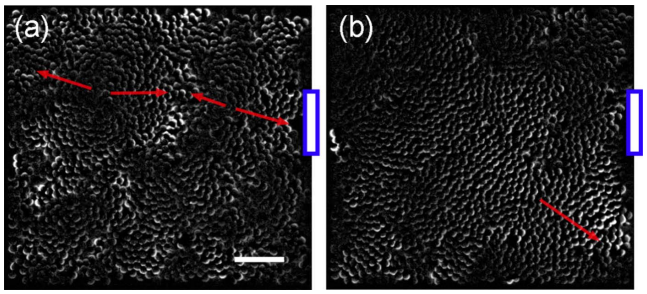

FIG. 15. (Color online) Displacement field of an inhomogeneous system in the smaller cell (16.5×16.5 cm^2). (a) Displacement field near the first peak of $g_1(\phi)$ at point (i) shown in Fig. 14. (b) Displacement field at the valley between the first and the second peaks at point (ii) shown in Fig. 14. The time interval for the displacement is $\Delta t = 800$ s. Red arrows show the local mean displacement. The blue box on the right indicates the force sensor at the boundary of the cell. The white scale bar is 3 cm.

and then it jams globally. For any system like this, depending on where the force sensor is located, the pressure measured may deviate from zero at different packing fractions. But it should always happen before the global jamming point (ϕ_2), as confirmed by the experiments.

With frictionless particles, the system can only jam as a whole due to force balance throughout the entire sample. Therefore, the multiple jamming points found in the system have to be due to friction between particles and between the particles and the boundary of cell. A frictional granular system can form very inhomogeneous structures such as force chains along one specific direction and jam in that direction, but still have empty space in other directions. As the size of particles increases further, force chains will buckle under the increasing stress, displacing particles into the less dense regions adjacent to the chains and causing the system to unjam. As a result, the system approaches the transition to jamming in a series of steps. This picture is reminiscent of the scenario proposed based on theoretical considerations that rigidity emerges by successive buckling of force chains in glasses and granular matter [40,41]. It should be emphasized that frictional contact is an essential ingredient for the existence of force chains before the global jamming point. However, deep inside the jammed phase, where the rigidity is already well established, force chains can sustain without friction. In conclusion, with friction the picture of a single jamming transition at $T=0$ [Fig. 1] has to be modified. Multiple jamming points may exist in a frictional system when a highly inhomogeneous structure is present.

To further test the above picture, we performed the experiment with small vertical vibrations applied to the system (Fig. 3). By vibrating the system, any force chains formed before jamming are destroyed by relative slip between particles. The vibration also helps one to demobilize the frictional contact between particles. If our picture of the relation between friction and jamming transition is correct, then by adding vibration the system should jam in one single step. In the experiment, the vibration is generated by a mechanical shaker in a tapping mode. Each tap is excited by one full period of a sinusoidal wave with the frequency $\omega = 30$ Hz.

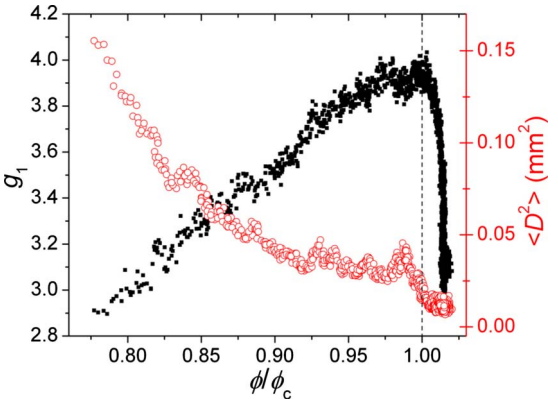

FIG. 16. (Color online) Structural signature of the jamming transition of a system subjected to small amplitude vibrations. The height of the first peak of pair correlation function g_1 is shown on the left with black squares. The mean-square displacement of particles $\langle D^2(\phi)\rangle$ is shown on the right with red circles. The time interval for the displacement is $\Delta t=200$ s. ϕ is normalized by the packing fraction at the jamming point $\phi_c \simeq 0.83$, which is indicated by the vertical dashed line.

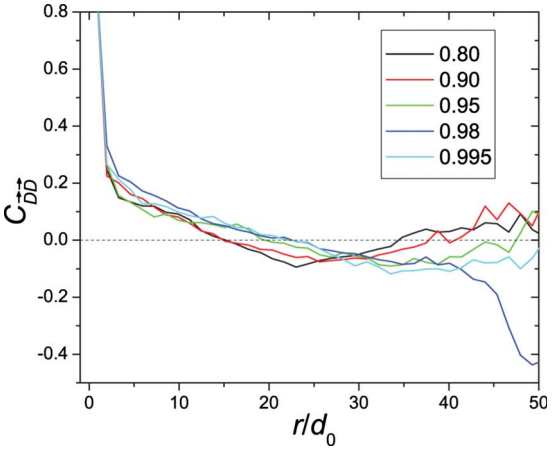

FIG. 17. (Color online) Correlation of the displacement of particles, $C_{\vec{D}\vec{D}}(r)$, for a system under vibration. Values of ϕ/ϕ_c are shown in the plots. Dashed horizontal line indicates zero correlation.

The peak-to-peak acceleration of vibration is $\Gamma_{p-p}=1.51g$, measured by an accelerometer attached to the cell. Here, g is the gravitational acceleration. The amplitude of vibration $A=\Gamma_{p-p}/(2\omega^2)=0.84$ mm is much smaller than the diameter of particles. Hence, particles only vibrate locally around their mean position. We tapped the cell once every 20 s before taking an image. A time interval of 2 s is allowed between shaking and taking an image, so the system is stationary when the image is taken. Six different experiments all with low initial packing fractions are performed. As expected, none of the experiments shows the multiple-step jamming. All the systems show a single peak in $g_1(\phi)$. We show a typical result in Fig. 16. Different from the results without vibration [Fig. 8(c)], the mean-square displacement of particles, $\langle D^2(\phi)\rangle$, decays monotonically [Fig. 16]. At low packing fraction, particles have more free room to vibrate and therefore have larger amplitude of displacement. The displacement amplitude decreases as the packing fraction of system increases and goes to zero when the system jams. Furthermore, the system under vibration does not develop any cluster structure as it approaches the jamming point. As shown in Fig. 17, the correlation of the displacement of particles, $C_{\vec{D}\vec{D}}(r)$, keeps roughly the same shape as $\phi \to \phi_c$, which is clearly different from the nonvibrating case. When the cluster structure develops, $C_{\vec{D}\vec{D}}(r)$ increases significantly [Fig. 11]. This confirms the argument that the cluster structure, and therefore the static length scale of the jamming transition, is due to the athermal nature of the system. Vibration thermalizes the system in a certain sense and therefore destroys the cluster structure.

VI. CONCLUSIONS

In this paper, we systematically investigate the jamming transition in a 2D granular system. We show that there is a clear structural signature of the jamming transition at zero temperature. The heights of the first and second peaks of the pair correlation function, $g_1(\phi)$ and $g_2(\phi)$, both show a maximum as the system crosses the jamming point. By measuring the pressure along the boundary and the displacement of particles, we show that this maximum coincides with the mechanical and kinematic criteria of jamming. Therefore, the structural signature we found here is a signature of the jamming transition. Although the amplitude of the peak does not diverge due to the polydispersity of our particles, our experiment corroborates the results predicted in simulations with ideal frictionless particles at zero temperature [9]. This signature has already been used as a new criterion of jamming at finite temperature, where the mechanical and kinematic criteria of jamming are hard to measure directly [18]. Here, our measurement which shows the coincidence of the maximum with the onset of the rigidity provides an experimental basis for the criterion. Of particular importance is that this structural signature exists for real granular systems with frictional contacts. The structural signature found in experiments reflects the underlying singularity of the jamming transition.

Friction may cause systems to jam in a series of steps. We found that if the initial packing configuration is highly inhomogenous, the system may jam in a certain direction but not in others. This phenomenon is directly related to the well-known force chain structure of a granular system [5]. Our observation provides more insight on the relation between the heterogeneous force-chain structure and the jamming transition in the presence of friction [40–42]. We speculate that the jamming transition of frictional system is obtained through a continuous buckling of force chains in the different directions.

It is also useful to note that $g_1(\phi)$ is a very sensitive probe for the jamming of system. Even partial jamming can induce a peak in $g_1(\phi)$. By contrast with the kinematic criterion of jamming, the average displacement or velocity of particles drops to zero only at the final global jamming point. For the mechanical criterion of jamming, depending on where one measures the pressure along the boundary, it may show

jamming at different packing fractions. Therefore, the peak of $g_1(\phi)$, which can be called the geometrical criterion, is a better jamming criterion for a system with friction.

Due to its athermal nature, this system has a dependence on its initial particle configuration. It amplifies any small initial density variation and self-organizes into clusters. A static length scale extracted from this cluster structure reaches the system size when the system approaches the jamming point. This static length scale is due to the nonequilibrium nature of the system. Hence, we show a divergent static length scale in this nonequilibrium jaming system.

ACKNOWLEDGMENTS

The author thanks S. Nagel and H. Jaeger for scientific guidance in discussions. I am grateful to E. Brown, N. Keim, J. Royer, N. Xu and L.-N. Zou for their help with the experiment and fruitful discussions. I also thank M. van Hecke for the careful reading of the original manuscript and many constructive comments and suggestions on the paper. This work was supported by the NSF MRSEC program under Contract No. DMR-0820054, by the Keck Initiative for Ultrafast Imaging at the University of Chicago, and by the DOE under Contract No. DE-FG02-03ER46088.

[1] P. W. Anderson, Science **267**, 1615 (1995).
[2] M. D. Ediger, C. A. Angell, and S. R. Nagel, J. Phys. Chem. **100**, 13200 (1996).
[3] A. Eisenberger, in *Physical Properties of Polymers* (American Chemical Society, Washington, D.C., 1984).
[4] E. R. Weeks, J. C. Crocker, A. C. Levitt, A. Schofield, and D. A. Weitz, Science **287**, 627 (2000).
[5] H. M. Jaeger, S. R. Nagel, and R. P. Behringer, Rev. Mod. Phys. **68**, 1259 (1996).
[6] A. J. Liu and S. R. Nagel, Nature (London) **396**, 21 (1998).
[7] C. S. O'Hern, L. E. Silbert, A. J. Liu, and S. R. Nagel, Phys. Rev. E **68**, 011306 (2003).
[8] L. E. Silbert, A. J. Liu, and S. R. Nagel, Phys. Rev. Lett. **95**, 098301 (2005).
[9] L. E. Silbert, A. J. Liu, and S. R. Nagel, Phys. Rev. E **73**, 041304 (2006).
[10] W. G. Ellenbroek, E. Somfai, M. van Hecke, and W. van Saarloos, Phys. Rev. Lett. **97**, 258001 (2006).
[11] E. Somfai, M. van Hecke, W. G. Ellenbroek, K. Shundyak, and W. van Saarloos, Phys. Rev. E **75**, 020301(R) (2007).
[12] K. Shundyak, M. van Hecke, and W. van Saarloos, Phys. Rev. E **75**, 010301(R) (2007).
[13] Z. Zeravcic, N. Xu, A. Liu, S. Nagel, and W. van Saarloos, EPL **87**, 26001 (2009).
[14] S. Henkes and B. Chakraborty, Phys. Rev. Lett. **95**, 198002 (2005).
[15] M. Mailman, C. F. Schreck, C. S. O'Hern, and B. Chakraborty, Phys. Rev. Lett. **102**, 255501 (2009).
[16] M. Wyart, S. R. Nagel, and T. A. Witten, EPL **72**, 486 (2005).
[17] M. Wyart, L. E. Silbert, S. R. Nagel, and T. A. Witten, Phys. Rev. E **72**, 051306 (2005).
[18] Z. Zhang, N. Xu, D. T. N. Chen, P. Yunker, A. M. Alsayed, K. B. Aptowicz, P. Habdas, A. J. Liu, S. R. Nagel, and A. G. Yodh, Nature (London) **459**, 230 (2009).
[19] N. Xu, e-print arXiv:0911.1576.
[20] T. S. Majmudar, M. Sperl, S. Luding, and R. P. Behringer, Phys. Rev. Lett. **98**, 058001 (2007).
[21] X. Jacob, V. Aleshin, V. Tournat, P. Leclaire, W. Lauriks, and V. E. Gusev, Phys. Rev. Lett. **100**, 158003 (2008).
[22] L. Bonneau, B. Andreotti, and E. Clément, Phys. Rev. Lett. **101**, 118001 (2008).
[23] E. I. Corwin, H. M. Jaeger, and S. R. Nagel, Nature (London) **435**, 1075 (2005).
[24] J. C. Crocker and D. G. Grier, J. Colloid Interface Sci. **179**, 298 (1996).
[25] O. Dauchot, G. Marty, and G. Biroli, Phys. Rev. Lett. **95**, 265701 (2005).
[26] F. Lechenault, O. Dauchot, G. Biroli, and J. P. Bouchaud, EPL **83**, 46003 (2008).
[27] A. S. Keys, A. R. Abate, S. C. Glotzer, and D. J. Durian, Nat. Phys. **3**, 260 (2007).
[28] S. Hales, *Statical Essays: Containing Vegetable Staticks* (Wilson and Nicol, England, 1769).
[29] R. Zallen, *The Physics of Amorphous Solids* (Wiley-VCH, Weinheim, 2004).
[30] H. P. Zhang and H. A. Makse, Phys. Rev. E **72**, 011301 (2005).
[31] L. E. Silbert, D. Ertas, G. S. Grest, T. C. Halsey, and D. Levine, Phys. Rev. E **65**, 031304 (2002).
[32] L. E. Busse and S. R. Nagel, Phys. Rev. Lett. **47**, 1848 (1981).
[33] D. Weaire and S. Hutzler, *The Physics of Foams* (Oxford University Press, Oxford, 1999).
[34] M. D. Ediger, Annu. Rev. Phys. Chem. **51**, 99 (2000).
[35] L. Berthier, G. Biroli, J.-P. Bouchaud, L. Cipelletti, D. El Masri, D. L'Hôte, F. Ladieu, and M. Pierno, Science **310**, 1797 (2005).
[36] W. K. Kegel and A. van Blaaderen, Science **287**, 290 (2000).
[37] K. Jonason, E. Vincent, J. Hammann, J. P. Bouchaud, and P. Nordblad, Phys. Rev. Lett. **81**, 3243 (1998).
[38] C. A. Angell, K. L. Ngai, G. B. McKenna, and P. F. McMillan, J. Appl. Phys. **88**, 3113 (2000).
[39] C. Josserand, A. V. Tkachenko, D. M. Mueth, and H. M. Jaeger, Phys. Rev. Lett. **85**, 3632 (2000).
[40] M. E. Cates, J. P. Wittmer, J.-P. Bouchaud, and P. Claudin, Phys. Rev. Lett. **81**, 1841 (1998).
[41] S. Alexander, Phys. Rep. **296**, 65 (1998).
[42] C. S. O'Hern, S. A. Langer, A. J. Liu, and S. R. Nagel, Phys. Rev. Lett. **86**, 111 (2001).